Progress in Organic Coatings 122 (2018) 88–95

Contents lists available at ScienceDirect

Progress in Organic Coatings

journal homepage: www.elsevier.com/locate/porgcoat

Fabrication of NCC-SiO_2 hybrid colloids and its application on waterborne poly(acrylic acid) coatings

Guomin Zhao, Chunxiang Ding, Mingzhu Pan*, Shengcheng Zhai

College of Materials Science and Engineering, Nanjing Forestry University, Nanjing 210037, China

ARTICLE INFO

Keywords:
Nanocrystalline cellulose
Waterborne poly(acrylic acid)
Abrasion resistance
Interface
Template

ABSTRACT

Nanocrystalline cellulose and nano SiO_2 (NCC-SiO_2) hybrid colloid was synthesized by *in situ* polymerization using a template of NCC. The prepared NCC-SiO_2 hybrid colloid was then introduced to waterborne poly acrylic acid (PAA) coatings. NCC template could inhibit an aggregation of nano SiO_2, leading to a uniform distribution of SiO_2 in PAA coatings. Furthermore, a formation of crosslink network of hydrogen bonding improved interfacial compatibility in a system of NCC, SiO_2 and PAA. Compared to the individual NCC and nano SiO_2, NCC-SiO_2 hybrid colloid had an obvious improvement on the mechanical performance and the transmittance of waterborne PAA coatings. With 5 wt% NCC-SiO_2 hybrid colloid, PAA coating had maximum mechanical properties, with corresponding to 6H in hardness, and level-0 in adhesion, respectively. Moreover, PAA coatings with 5 wt% NCC-SiO_2 hybrid colloid had a higher transmittance of 41.8% at 390 nm.

1. Introduction

Waterborne poly(acrylic acid) (PAA) coating has been widely used in wood furniture finishing, glass coating, and automotive finishing due to its environmental friendly, corrosion resistance, alkali resistance, and suitable film-forming [1,2]. However, its practical industrial applications in interior wood and glass coating are often limited for its weak abrasion resistance, low transmittance and short lifetime [3,4]. In order to improve the abrasion resistance of waterborne PAA coatings, the inorganic nanoparticles or metallic oxide, such as nano SiO_2, nano zirconia and nano aluminum oxide, are always introduced to provide high hardness, strong heat-stable, and low-cost synthesis [5–8].

Introducing nano SiO_2 to PAA coatings is one of the important modifications on abrasion resistance of PAA coating. Norouzi et al. [9] added the polyhedral oligomeric silsesquioxane (POSS) to acrylic acid with esterification reaction. With increasing POSS content, POSS-acrylate composite coatings showed a higher abrasion resistance, and the abrasion resistance index of POSS-acrylate composite coating had a maximum value with 5 wt% POSS. However, the transmittance of POSS-acrylate composite coating gradually decreased from 90% to 85%. Sow et al. [10] embedded silica nanoparticles into UV-waterborne polyurethane-acrylate (PU-acrylate) nanocomposite coatings. With increasing nano silica to 1 wt%, the abrasion resistance of PU-acrylate nanocomposite coatings increased from 22% to 71%. The adhesion of PU-acrylate nanocomposite coatings increased from 6.4 MPa to 8.8 MPa, and its glass transition temperature increased from 64°C to 78 °C, respectively. Furthermore, the transmittance of PU-acrylate nanocomposite coatings significantly reduced from 100% to 38%. Jindasuwan et al. [11] assembled poly allylamine hydrochloride/poly acrylic acid (PAH/PAA)/nano SiO_2 coating using a layer-by-layer method. The addition of nano SiO_2 increased surface roughness of PAH/PAA coating from 5.0 nm to 60.2 nm. The adhesion of PAH/PAA coating also increased from level-4 to level-3. However, PAH/PAA coating had a 3.1% reduction in transmittance. These reports show that the addition of nano SiO_2 clearly served to achieve a higher surface roughness and abrasion resistance of PAA coatings. However, it decreased the transmittance of PAA coatings due to an aggregation of nano SiO_2 in polymer coating.

Cellulose, consisting of repeating D-glucose units, is the most abundant organic polymer all around the word [12]. Nanocrystalline cellulose (NCC), which is always derived from cellulosic materials, has superior properties such as low axial thermal expansion coefficient of 10^{-7} k^{-1}, high aspect ratio of 150–1000 $m^2 \cdot g^{-1}$, extraordinary modulus of 70–150 GPa [13]. Moreover, NCC is commonly obtained by acid hydrolysis, has a rod-shaped structural with 10 nm to 20 nm in diameter and several hundred nanometers in length [14], and it has chiral liquid crystal alignment structures and hydroxyl groups [15]. Due to its excellent performance, NCC has been attractively considered for a template of NCC-inorganic composite materials. Shin and Exarhos [16] successfully constructed porous titania including mesopores using NCC template. Zhou et al. [17] prepared cube-shaped TiO_2 nanoparticles with a high crystallinity and uniform size by a template of NCC.

* Corresponding author.
E-mail address: mzpan@njfu.edu.cn (M. Pan).

https://doi.org/10.1016/j.porgcoat.2018.05.014
Received 5 December 2017; Received in revised form 3 May 2018; Accepted 9 May 2018

Shopsowitz et al. [18] fabricated free-standing mesoporous silica films with tunable chiral nematic structures by a template of NCC. Song et al. [19] synthesized mesoporous silica nanotubes with dual templates of cetyltrimethylammonium bromide (CTAB) and NCC. The template of NCC promoted a uniform dispersion of SiO_2 on the surface of NCC. NCC-SiO_2 hybrid colloid combined an excellent reinforcement of NCC and high thermal stability, high hardness, and photoelectric effect of SiO_2, comparing with the individual NCC and nano SiO_2. Myoug et al. [20] added acetylated cellulose nanocrystals (ACN)/silica nanocomposites to poly(lactide) (PLA). The dispersion of silica was improved in PLA/ACN/silica nanocomposites, which significantly improved the thermal property and crystallinity. Zhang et al. [21] reported that polystyrene (PS) with 5 wt% of NCC-SiO_2 had a tensile strength of 110 MPa, and an Izod notched impact strength of 5.00 $KJ{\cdot}m^{-2}$, respectively, which increased by about three times and eight times compared than that of pure PS.

Moreover, NCC and NCC/inorganic compounds have been introduced to enhance waterborne coatings due to its unique reinforcement. El-Fattah et al. [22] added NCC to waterborne PU coating, and pointed that an optimum mechanical property was present in PU with 1.5 wt % NCC. Vardanyan et al. [23] modified NCC with alkyl quaternary ammonium bromides and acryloyl chloride, and then added the modified NCC to UV-waterborne coatings. The modified NCC resulted in an approximately 30–40% in abrasion resistance of UV-waterborne coatings. In this paper, we prepared NCC-SiO_2 hybrid colloid through *in situ* polymerization using a template of NCC. The prepared NCC-SiO_2 hybrid colloid was then introduced to waterborne PAA coatings. The properties of PAA coating with NCC-SiO_2 hybrid colloid were investigated with atomic force microscope (AFM), field-emission scanning electron microscope (FE-SEM), Fourier infrared spectra (FTIR), and x-ray diffraction (XRD) measurements. The possible mechanism of abrasion resistance of PAA coating with NCC-SiO_2 hybrid colloid was also proposed in this paper.

2. Experimental

2.1. Materials

Waterborne PAA with main component of acrylic resin (solid content of 42 wt%) was supplied by Tikkurila Paints Co., Ltd. (Beijing, China). Microcrystalline cellulose (MCC) power (~50 μm in diameter) was kindly provided by Shanhe Pharmaceutical Excipients Co., Ltd. (Anhui, China). Ethyl silicate (TEOS, 25% SiO_2), H_2SO_4 (95%–98%), ammonia solution (25%-28%), and ethanol (≥99.7%) with analytical grade were obtained from Sinopharm Chemical Reagent Co., Ltd. (Nanjing, China). All chemical agents were used without further purification.

2.2. Preparation of NCC-SiO_2 hybrid colloid

NCC was prepared according to our previous study [24]. About 10 *g* MCC was hydrolyzed with 98 mL of 64 wt% sulfuric acid at 44 °C for 2 *h*. The suspension was then diluted 10-fold to stop the reaction, and diluted with the deionized water and centrifuged for 5 times. The sample was dialyzed for 3 days until the pH of the supernatant was neutral. Subsequently, the colloidal solution was homogenized using a high-pressure homogenizer (AH100D, USA) with 500 bar for 5 times to obtain NCC suspension. And then, NCC suspension was condensed using a rotary evaporator until NCC concentration reached 0.8 wt%.

NCC-SiO_2 hybrid colloid was prepared by sol-gel method. 96 g of above-prepared 0.8 wt% NCC, 46.2 μL TEOS, and 43.8 μL ethanol were placed into a 250 mL rounded bottom flask, and then stirred with 250 rpm at 65 °C for 2 h. Afterwards, the ammonia solution was added to adjust the pH value of reaction system to 9. The reaction system was continued to stir with 250 rpm at 80 °C for 2 h to obtain NCC-SiO_2 hybrid colloid. Nano SiO_2 was also synthesized with a similar procedure by dropping 23.1 mL TEOS, 21.9 mL ethanol, and 3.8 mL deionized water into a 100 mL rounded bottom flask.

2.3. Preparation of waterborne PAA coatings

16 g PAA was placed in a 100 mL rounded bottom flask. NCC-SiO_2 hybrid colloid as above-mentioned prepared was firstly sonicated with 90 W for 15 min, and then added to PAA. The addition of NCC-SiO_2 hybrid colloid was 1, 2, 3, 4, 5, 6, and 7 wt% (solid weight based on solid weight of PAA coating), respectively. The mixtures were stirred with 500 rpm at 25 °C for 1h to obtain homogeneous compounds. Subsequently, the compounds were coated on the surface of clean glass with 5 mm × 12 mm, and air-dried for 3 days to obtain coating films, which had a thickness of 175–190 μm and a moisture content of 2.5 wt %. For comparison, PAA coating was individually treated with 5 wt% NCC or 5 wt% nano SiO_2.

2.4. Characterizations

The morphology of NCC, nano SiO_2 and NCC-SiO_2 hybrid colloid was observed with transmission electron microscope (TEM, JEM-1400, JEOL) at 100 kV. The suspension was diluted to 0.1 wt% and deposited onto carbon-coated grids (300-mesh copper) before measurement.

X-ray diffraction (XRD) was performed to investigate the phase structure of NCC, nano SiO_2, and NCC-SiO_2 hybrid colloid. The samples were flatted into pellets between two glass slides and placed in an Ultima IV diffractometer (Rigaku, Japan) with Cu K_α radiation (λ = 0.15406 nm), operating at 40 kV and 30 mA. The diffraction profile was detected by using a locked couple 2θ scan from 5 to 50°.

Fourier-infrared (FTIR) spectra were recorded by a VERTEX 80 infrared spectrum instrument (Bruker, Germany). Samples of NCC, nano SiO_2 and NCC-SiO_2 hybrid colloid were firstly freeze-dried. And then, samples and KBr powder were uniformly ground and pressed to form pellet. The spectra of samples were recorded within a range of 4000-400 cm^{-1} with a resolution of 0.5 cm^{-1}.

Thermogravimetric (TG) measurement was carried out on a NETZSCH TG 209 F3 (Netzsch, Germany) in a continuous nitrogen atmosphere at a heating rate of 10 °C/min from 35 to 700 °C. 3–4 mg of sample was used for TG testing.

The surface of PAA coatings with and without modification was observed with atomic force microscope (AFM, Dimesion Edge, Bruker, Germany) using a tapping mode of silicon probes under a 1 Hz scan rate, and 512 pixels × 512 pixels image resolution. The average surface roughness was determined from AFM height images of PAA coatings.

The fracture surface of PAA coatings with and without modification was characterized by a field-emission scanning electron microscope (FE-SEM, HITACHI S4800, Thermo Scientific, USA). Samples were firstly fractured in liquid nitrogen, and then coated with gold before examination at 15 kV.

UV–vis absorption spectra of waterborne PAA coatings with and without modification were measured by a UV–vis spectrophotometer (Lambda 950, PE, USA). In order to clearly demonstrate the transmittance of waterborne PAA coatings, the spectra of samples were continuously recorded within UV light in a range of 250–390 nm, and the visible light in a range of 390–800 nm with a resolution of 0.08 nm.

Hardness and adhesion are important parameters to reflect the abrasion resistance of coating [25]. The hardness and adhesion of waterborne PAA coatings with and without modification were determined according to National Standards of the People's Republic of China GB/T 6739-2006, and GB/T 1720–2006, respectively, which are technically equivalent to ASTM D3363-2005, and ASTM D3359-2009 standard tests. In brief, for hardness measurement, set of wooden drawing pencils were used with hardness of 2B, B, HB, H, 2H, 3H, 4H, 5H, and 6H. For adhesion measurement, 3 M Scotch tape was used for evaluation of adhesion of coatings. Adhesion is standard of level-0, level-1, level-2, level-3, and level-4. The strength of adhesion is order of level-

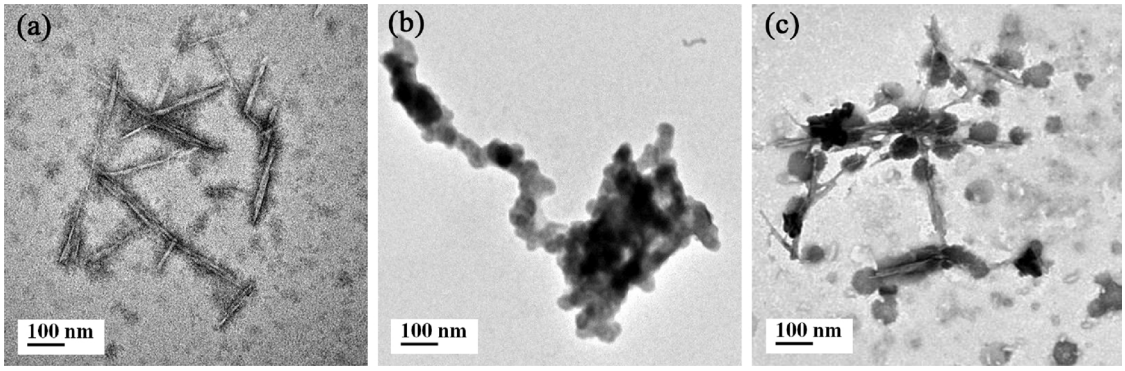

Fig. 1. TEM images of (a) NCC, (b) nano SiO_2, and (c) NCC-SiO_2 hybrid colloid.

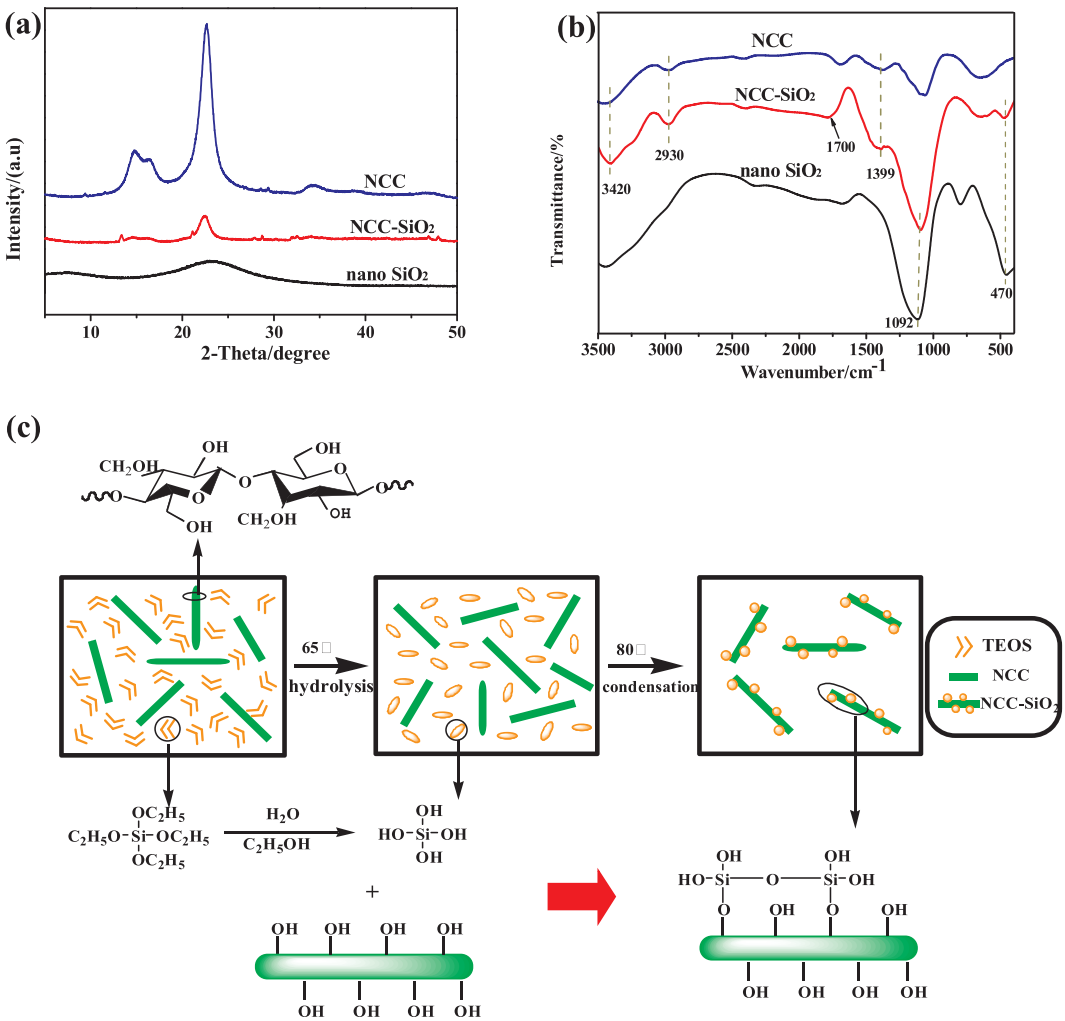

Fig. 2. Characteristics of NCC, nano SiO_2, and NCC-SiO_2 hybrid colloid: (a) XRD profiles, (b) FTIR spectra, and (c) possible schematic illustraion of NCC-SiO_2 hybrid colloid.

0 > level-1 > level-2 > level-3 > level-4. Six different positions were performed in each sample. All the samples were tested at 25 ± 2 °C.

3. Results and discussion

3.1. Characteristics of NCC-SiO_2 hybrid colloid

Fig. 1 shows TEM images of NCC, nano-SiO_2, and NCC-SiO_2 hybrid colloid. NCC exhibited a typical rod-shaped crystal with a diameter of 5–10 nm and a length of 100-200 nm (Fig. 1(a)). Nano SiO_2 showed the homogeneous granules with aggregation (Fig. 1(b)). NCC-SiO_2 hybrid colloid had a combined morphological characteristic, wherein nano SiO_2 clustered uniformly on surface of NCC (Fig. 1(c)). During sol-gel of TEOS, partial hydroxyl groups of NCC *in situ* polymerized with sol of nano SiO_2, leading to a formation of nano SiO_2 on the surface of NCC. Additionally, hydroxyl groups present on the surface of NCC could also act as a stabilizer for nano SiO_2. It revealed that NCC exhibited a template effect during sol-gel of TEOS, promoting a uniform distribution of nano SiO_2 on the surface of NCC.

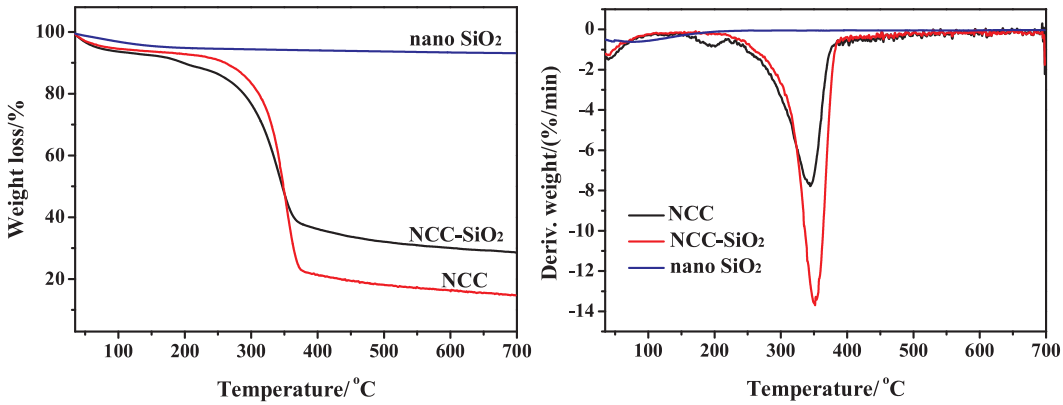

Fig. 3. TG and DTG curves of NCC, nano SiO_2, and NCC-SiO_2 hybrid colloid.

Table 1
TG results of NCC-SiO_2 hybrid colloid under a nitrogen atmosphere.

Samples	$T_{5\%}$ (°C)	T_{peak} (°C)	Mass loss at T_{peak} (wt%)	Residual mass at 700 °C (wt%)
NCC	96.4	343.7	52.55	14.82
Nano SiO_2	204.1	–	–	93.35
NCC-SiO_2	93.8	352.6	44.51	28.94

Fig. 2(a) shows XRD profiles of NCC, nano SiO_2, and NCC-SiO_2 hybrid colloid. NCC showed characteristic diffraction peaks at 2θ values of 14.63°, 16.23°, 22.49°, and 34.31°, respectively, which can be assigned to crystalline planes with Miller indices of [-101], [101] [002], and [040] for cellulose *I* [26,27]. Nano SiO_2 exhibited a broad peak at about 22°, attributing to an amorphous phase of nano SiO_2. NCC-SiO_2 hybrid colloid had the characteristic diffraction peaks at 2θ value of 22.49°, indicating NCC remained crystalline planes of cellulose*I*- during gel-sol process of TEOS. Furthermore, the minor peaks appeared at 13.37° and 21.13° were attributed to [-101] and [020] lattice planes of cellulose *II* of NCC [28]. It revealed that the crystalline structure of NCC partially converted from cellulose *I* to cellulose *II* in presence of ammonia during sol-gel process. This finding was in agreement with a previous research by Qu et al. [29].

Fig. 2(b) presents FTIR spectra of NCC, nano-SiO_2, and NCC-SiO_2 hybrid colloid. For NCC, the peaks at 3420, 2930 and 1399 cm^{-1} were assigned to the stretching of hydroxyl groups (−OH), the aliphatic

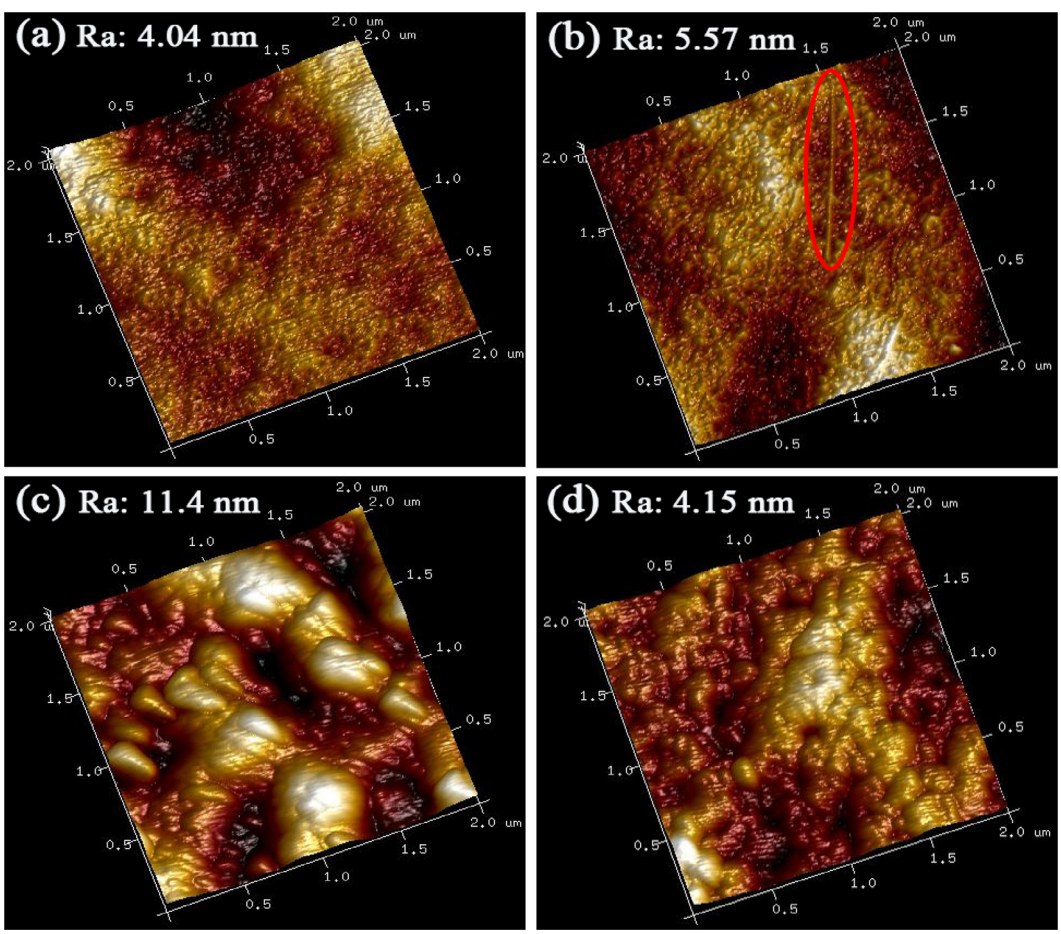

Fig. 4. AFM-micrographs (3D) of the surface of coatings: (a) PAA, (b) PAA/NCC 5 wt%, (c) PAA/nano SiO_2 5 wt%, and (d) PAA/NCC-SiO_2 5 wt%.

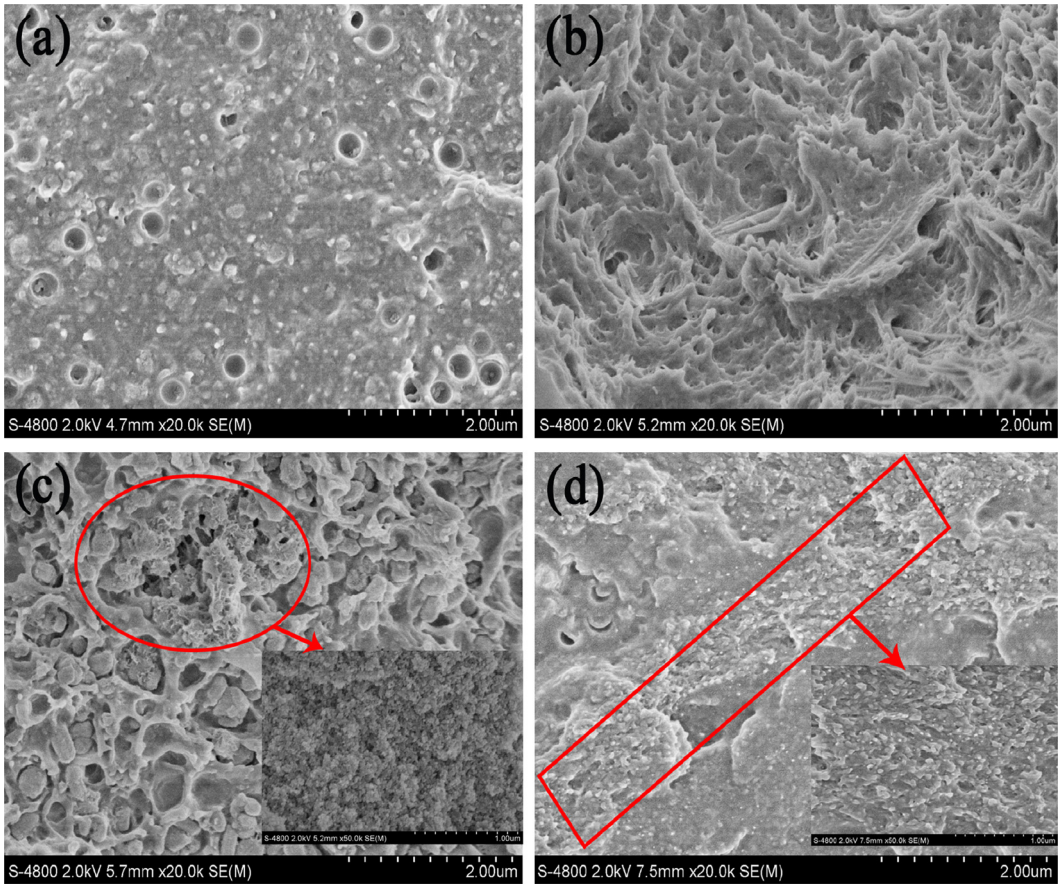

Fig. 5. FE-SEM photographs of the fracture surface of coatings: (a) PAA, (b) PAA/NCC 5 wt%, (c) PAA/nano SiO_2 5 wt%, and (d) PAA/NCC-SiO_2 5 wt%.

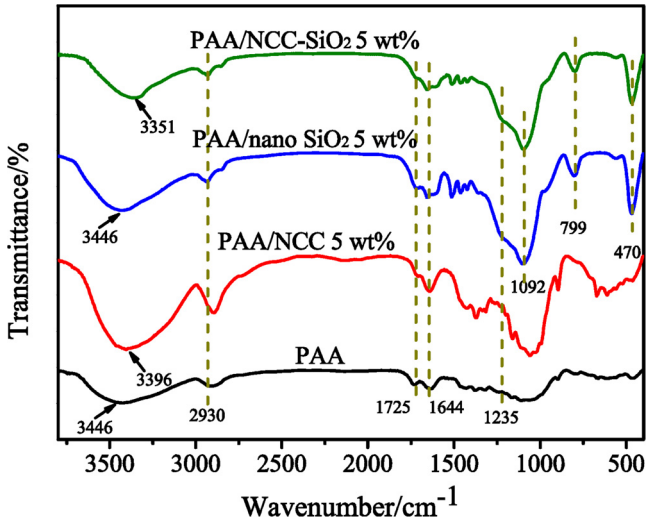

Fig. 6. FTIR spectra of waterborne PAA coatings with and without modification.

saturated C—H stretching vibration, and C—H bending bands, respectively [30,31]. For nano SiO_2, the peaks at 1092 and 470 cm^{-1} were assigned to Si-O-Si, and O-Si-O bending modes of bridging oxygen, respectively [32]. For NCC-SiO_2 hybrid colloid, it exhibited a combined characteristic band of NCC and nano SiO_2. Furthermore, a new absorption peak was appeared at 1700 cm^{-1}, which was assigned to C—O—Si. A possible hypothesis of NCC—SiO_2 hybrid colloid is proposed according the above results. During hydrolysis of TEOS, the $SiOC_2H_5$ group was firstly transformed into Si—OH. Subsequently, Si—OH reacted with —OH of NCC, leading to a formation of C-O-Si. It induced a uniform distribution of nano SiO_2 on the surface of NCC, which was proved by TEM (Fig. 1(c)). Moreover, Si-O-Si was partially formed by self-condensation reaction of Si—OH. Possible reactions between NCC and nano SiO_2 are shown in Fig. 2(c).

Fig. 3 shows TG and its derivative thermogravimetry (DTG) curves for NCC, nano SiO_2, and NCC-SiO_2 hybrid colloid. The onset temperature ($T_{5\%}$), the peak decomposition temperature (T_{peak}), the mass loss at T_{peak}, and the residual mass at 700 °C are presented in Table 1. For NCC, $T_{5\%}$ and T_{peak} appeared at 96.4 °C and 343.7 °C, respectively. The residual mass of NCC was 14.82 wt%. Compared to NCC, nano SiO_2 showed a higher thermal stability, and the residual mass during the whole thermal degradation was rarely decreased. For NCC-SiO_2, $T_{5\%}$ had no obvious change with that of NCC, while, T_{peak} increased to 352.6 °C. The residual mass of NCC-SiO_2 was 28.94 wt%. Nano SiO_2 was reacted with hydroxyl groups of NCC, and then grafted into the surface of NCC, leading to a higher thermal stability of NCC-SiO_2 hybrid colloid than that of NCC.

3.2. Morphological analysis of PAA coatings

Fig. 4 shows the surface morphology of waterborne PAA coatings with and without modification. Neat PAA showed a uniform surface accompanying with quantities of minor protrusions due to intrinsic additive particles in PAA coating (Fig. 4(a)). The surface roughness of neat PAA coating was evaluated to 4.04 nm. For PAA/NCC 5 wt%, NCC distributed homogeneously and agglomerated randomly in the surface of coating film with a slightly higher surface roughness of 5.57 nm (Fig. 4(b)). However, for PAA/nano SiO_2 5 wt%, it showed an uneven surface with a significantly higher surface roughness of 11.4 nm (Fig. 4(c)). It is attributed to the aggregation of nano SiO_2 in coating

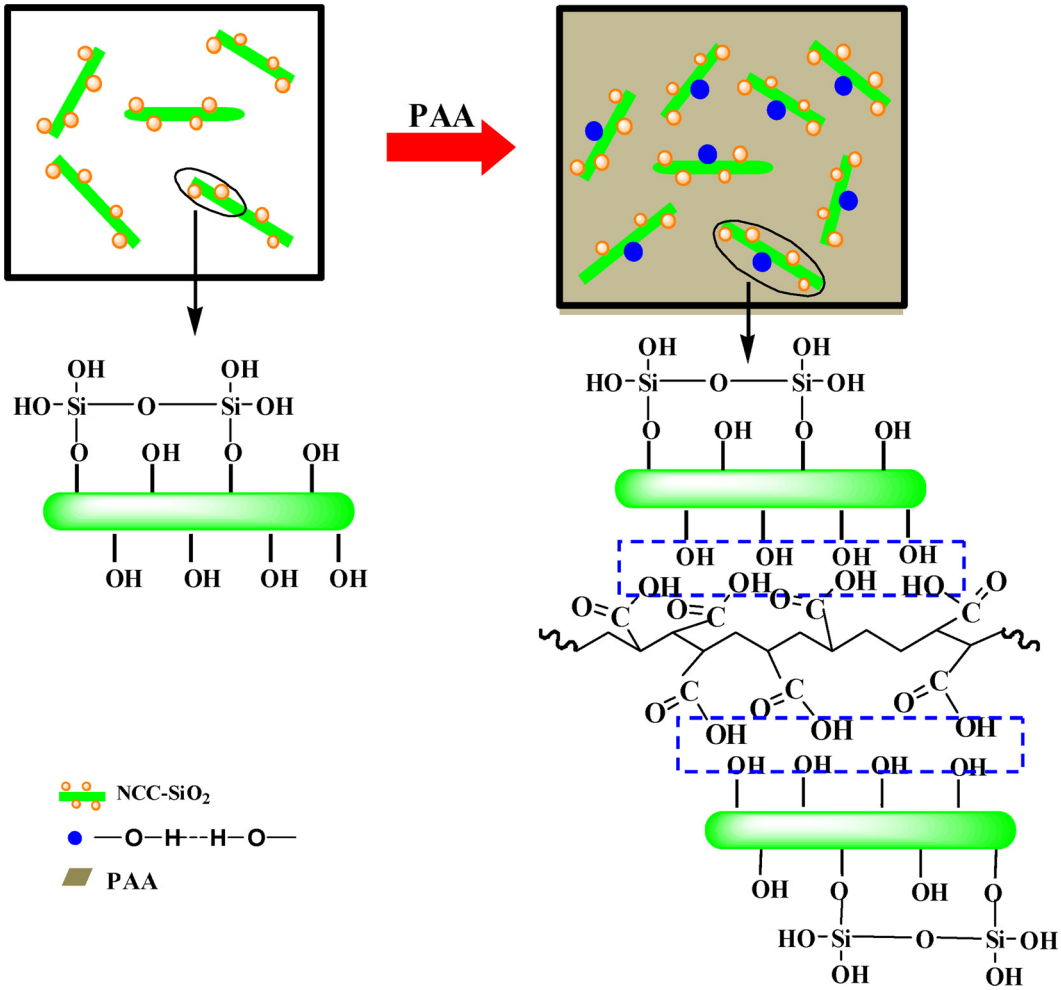

Fig. 7. Possible scheme of modification mechanism between NCC-SiO_2 and PAA coating.

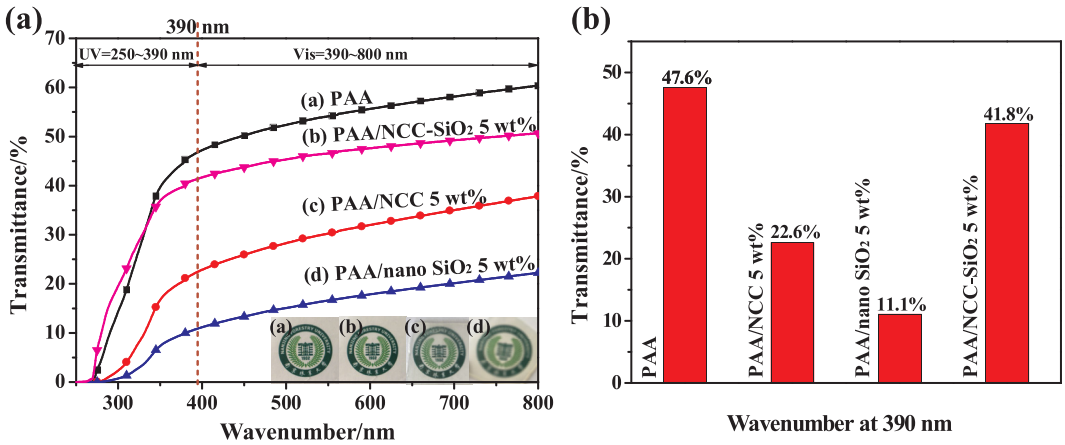

Fig. 8. UV–vis transmittance of waterborne PAA coatings with and without modification: (a) transmittance at 250–800 nm, (b) transmittance at 390 nm.

film. For PAA/NCC-SiO_2 5 wt%, it had a significant smooth surface with a surface roughness of 4.15 nm (Fig. 4(d)). It is probably due to that NCC-SiO_2 distributed more homogeneously in coating film with a template effect of NCC, which was further discussed in the following analysis.

Fig. 5 illustrates the fracture surface of waterborne PAA coatings with and without modification. For neat PAA, the fracture surfaces of coating film had some holes and white dots, due to the disorder arrangement of the intrinsic additive particles of PAA coatings (Fig. 5(a)). The loose network with holes and white dots could lower the hardness and abrasion resistance of PAA coating, which is proven by the mechanical test. For PAA/NCC 5 wt%, many holes disappeared in the fracture surfaces of coating film, the transversal section or pullout of NCC was also appeared (Fig. 5(b)). It revealed that the empty spaces between PAA and NCC became smaller and less, strengthening interfacial bonding between PAA and NCC. For PAA/nano SiO_2 5 wt%, nano SiO_2 granules (as shown in the red circles) were embedded in coating film accompanying with obvious gaps (Fig. 5(c)), due to the weak

Table 2
Mechanical properties of waterborne PAA coatings with and without modification.

Samples	Hardness[a]	Adhesion[b]
PAA	H (0)	level-4 (0)
PAA/NCC 5 wt%	3H (0)	level-2 (0)
PAA/nano SiO_2 5 wt%	3H (± 0.82)	level-2 (± 0.58)
PAA/NCC-SiO_2 1 wt%	2H (0)	level-3 (0)
PAA/NCC-SiO_2 2 wt%	3H (0)	level-2 (0)
PAA/NCC-SiO_2 3 wt%	4H (0)	level-1 (± 0.58)
PAA/NCC-SiO_2 4 wt%	5H (0)	level-1 (0)
PAA/NCC-SiO_2 5 wt%	6H (0)	level-0 (0)
PAA/NCC-SiO_2 6 wt%	6H (± 0.58)	level-1 (0)
PAA/NCC-SiO_2 7 wt%	6H (± 0.58)	level-2 (0)

Values in parentheses are the standard deviations of the six measurements.
[a] Hardness standard is in order of 6H > 5H > 4H > 3H > 2H > H.
[b] Adhesion standard is in order of level-0 > level-1 > level-2 > level-3 > level-4.

interfacial compatibility. For PAA/NCC-SiO_2 5 wt%, it is no obvious holes in the fracture surfaces of coating film. The fracture surface of coating film was more contact and continuous compared to that of PAA/NCC 5 wt% and PAA/nano SiO_2 5 wt%, exhibiting an improved interfacial bonding between PAA and SiO_2 in the presence of NCC (Fig. 5(d)). Moreover, NCC-SiO_2 hybrid particles (as pointed by red rectangle) distributed homogeneously in coating film with much more contact.

3.3. FTIR analysis of PAA coatings

Fig. 6 shows FTIR spectra of waterborne PAA coatings with and without modification. For neat PAA, the absorption band at 3500-3300 cm^{-1} was characteristic of −OH stretching, and the peak at 2930 cm^{-1} was C−H stretching vibration, respectively. The characteristic peaks at 1725 cm^{-1} and 1235 cm^{-1} were assigned to −C═O, and −C−O in carboxyl groups, respectively [33]. Another peak at 1644 cm^{-1} was assigned to C═C, which was the characteristic peak of PAA [10]. For PAA/NCC 5 wt%, the peak of hydroxyl groups shifted from 3446 $cm^{-1}$to 3396 cm^{-1}, due to a formation of hydrogen bonding between NCC and PAA [34]. For PAA/nano SiO_2 5 wt%, it only exhibited characteristic peaks of PAA and nano SiO_2. For PAA/NCC-SiO_2 5 wt%, the peak of hydroxyl groups had a red shift of 95 cm^{-1}, and it revealed that the inter hydrogen bonding was formed between PAA and NCC-SiO_2. Fig. 7 illustrates a hypothesis of possible modification mechanism between NCC-SiO_2 and PAA coating. The hydroxyl groups from the molecular of PAA, NCC, and nano SiO_2 could react each other, leading to crosslinked networks of hydrogen bonding. It further improved interfacial compatibility in a system of PAA, NCC, and SiO_2, promoting a uniform distribution of SiO_2 in PAA coating in a presence of NCC template, which is proven from Figs. 4(d) and 5(d).

3.4. UV–vis spectroscopy analysis

Fig. 8(a) presents the results of UV–vis spectroscopy of waterborne PAA coatings with and without modification, and the inset photographs shows coating films placed on a background paper to demonstrate their transmittance. As shown in Fig. 8(a), the transmittance of waterborne PAA coating films increased with increasing the wavenumber from UV light of 250–390 nm to visible light of 390–800 nm. Fig. 8(b) clearly presents the transmittance of waterborne PAA coating films at 390 nm. For neat PAA coating, the transmittance was 47.6% at 390 nm. For PAA/NCC 5 wt%, the transmittance decreased to 22.6%. It was probably due to a partial aggregation of NCC, which was shown in Fig. 4(b). It indicated that the scattering of aggregated domains lead to a loss of transmittance, which was in agreement with the previous research by Chang et al. [35]. For PAA/nano SiO_2 5 wt%, the transmittance significantly decreased to 11.1%, due to the severer aggregation of nano SiO_2, which was shown in Fig. 4(c). Additionally, amounts of nano SiO_2 in PAA/ nano SiO_2 5 wt% was larger compared to that in PAA/NCC-SiO_2 5 wt%. It was further proven an obviously decreased transmittance of PAA/nano SiO_2 5 wt%. In contrast, for PAA/NCC-SiO_2 5 wt%, the transmittance significantly increased to 41.8%. It was higher than that of PAA/nano SiO_2 5 wt%, and slightly lower than that of neat PAA. It is due to a uniform distribution of NCC-SiO_2 in PAA, which was proven by the morphological analysis and FTIR results.

3.5. Mechanical properties analysis

The mechanical performance of coatings is of great importance for its practical application. Table 2 summarizes the hardness and adhesion of waterborne PAA coatings with and without modification. Neat PAA showed a hardness and adhesion of H and level-4. For PAA/NCC 5 wt%, the hardness and adhesion were 3H and level-2, respectively. The improvement was related to an arrangement of NCC within PAA matrix and the interactions between NCC and PAA molecules. The formation of hydrogen bonding played a bridging role between NCC and PAA, and it promoted the hardness and adhesion of PAA/NCC coating [36,37]. For PAA/nano SiO_2 5 wt%, the hardness and adhesion remained 3H and level-2, which was higher than that of neat PAA coating. It is probably attributed to the high hardness of nano SiO_2. However, PAA/nano SiO_2 5 wt% had an unstable hardness and adhesion in the measurement positions. It is due to the uneven distribution of nano SiO_2 in PAA coating.

As expected, for all samples of PAA/NCC-SiO_2 coating, the hardness and adhesion were higher than that of neat PAA coating. In particular, the hardness and adhesion of PAA/NCC-SiO_2 coating increased gradually with increasing the content of NCC-SiO_2. It reached a maximum of hardness and adhesion of 6H and level-0 at the content of 5 wt% NCC-SiO_2, which is similar to that of PAA/NCC coating. The modification on PAA coating may induce two effects: (1) NCC-SiO_2 interacts with PAA molecules through hydrogen bonding in PAA/NCC-SiO_2 coating. (2) A template of NCC restricts the aggregation of nano SiO_2, leading to promote the uniform distribution of NCC-SiO_2 in PAA/NCC-SiO_2 coating. However, PAA/NCC-SiO_2 coating had a trend of decrease on the hardness and adhesion with increasing the content of NCC-SiO_2 up 5 wt%. For PAA/NCC-SiO_2 7 wt%, the hardness and adhesion reduced to 6H and level-2, respectively. It is probably that higher content of NCC-SiO_2 hybrid colloids could induce an obvious aggregation in PAA matrix. Furthermore, it could reduce a formation of inter hydrogen bonding between NCC-SiO_2 and PAA, leading to a reduction of crosslink network of hydrogen bonding between NCC-SiO_2 and PAA. The interaction between NCC-SiO_2 and PAA was thus weakened. Consequently, the mechanical performance of PAA/NCC-SiO_2 coating decreased gradually.

4. Conclusions

NCC-SiO_2 hybrid colloid was synthesized *via in situ* polymerization with a template of NCC. The prepared NCC-SiO_2 hybrid colloid was then modified the waterborne PAA coatings. NCC template could restrict an aggregation of nano SiO_2, leading to a uniform distribution of SiO_2 in PAA coatings. Furthermore, a formation of crosslink network of hydrogen bonding improved the interfacial compatibility in a system of NCC, SiO_2 and PAA. Synergetic effects of a uniform distribution and interfacial compatibility could improve the surface roughness and transmittance of waterborne PAA coatings. With 5 wt% NCC-SiO_2 hybrid colloid, PAA coating had a significant smooth surface with a surface roughness of 4.15 nm, and increased a transmittance to 41.8% at 390 nm. Moreover, PAA coatings with 5 wt% NCC-SiO_2 hybrid colloid PAA coating had a maximum mechanical performance, with corresponding to 6H in hardness, and level-0 in adhesion, respectively.

Acknowledgements

This study was supported by National Natural Science Foundation of China (Grant No. 31670556, 31400496), Science Fund for Distinguished Young Scholars of Nanjing Forestry University (Grant No. NLJQ2015-02) and a Project Funded by the Priority Academic Program Development of Jiangsu Higher Education Institutions (PAPD). The authors thank Depei Zhang and Wendi Li for their technical assistance.

References

[1] Q. Chen, H.J. Yu, L. Wang, Synthesis and characterization of amylose grafted poly (acrylic acid) and its application in ammonia adsorption, Carbohyd. Polym. 153 (2016) 429–434.
[2] L. Weng, H.X. Li, X.P. Yang, L.Z. Liu, Preparation and characterization of silica/polyimide nanocomposite films based on water-soluble poly(amic acid) ammonium salt, Polym. Composite 38 (2017) 774–781.
[3] F. Bauer, H.J. Gläsela, U. Deckera, H. Ernstb, A. Freyera, E. Hartmanna, V. Sauerlandc, R. Mehnert, Trialkoxysilane grafting onto nanoparticles for the preparation of clear coat polyacrylate systems with excellent scratch performance, Prog. Org. Coat. 47 (2003) 147–153.
[4] A. Bauer, D. Meinderink, I. Giner, H. Steger, J. Weitl, G. Grundmeier, Electropolymerization of acrylic acid on carbon fibers for improved epoxy/fiber adhesion, Surf. Coat. Tech. 321 (2017) 128–135.
[5] K. Xu, S.X. Zhou, L.M. Wu, Dispersion of γ-methacryloxypropyltrimethoxysilane functionalized zirconia nanoparticles in UV-curable formulations and properties of their cured coatings, Prog. Org. Coat. 67 (2010) 302–310.
[6] M. Wang, X. Li, W.K. Hua, L.D. Shen, X.F. Yu, X.F. Wang, Electrospun poly(acrylic acid)/silica hydrogel nanofibers scaffold for highly efficient adsorption of lanthanide ions and its photoluminescence performance, ACS Appl. Mater. Interfaces 8 (2016) 23995–24007.
[7] C.H. Campos, B.F. Urbano, B.L. Rivas, Synthesis and characterization of organic-inorganic hybrid composites from poly(acrylic acid)-[3-(trimethoxysilyl)propyl methacrylate]-Al_2O_3, Compos. Part B-Eng. 57 (2014) 1–7.
[8] S. Cakić, G. Nikolić, Ć. Lačnjevac, M. Gligorić, M.B. Rajković, The thermal degradation of aqueous polyurethanes with catalysts of different selectivity, Prog. Org. Coat. 60 (2007) 112–116.
[9] S. Norouzi, M. Mohseni, H. Yahyaei, Preparation and characterization of an acrylic acid modified polyhedral oligomeric silsesquioxane and investigating its effect in a UV curable coating, Prog. Org. Coat. 99 (2016) 1–10.
[10] C. Sow, B. Riedl, P. Blanchet, UV-waterborne polyurethane-acrylate nanocomposite coatings containing alumina and silica nanoparticles for wood: mechanical, optical, and thermal properties assessment, J. Coat. Technol. Res. 8 (2011) 211–221.
[11] S. Jindasuwan, O. Nimittrakoolchai, S. Supothina, Surface property and stability of transparent superhydrophobic coating based on SiO_2-Polyelectrolyte multilayer, Mater. Sci-Medzg. 22 (2016) 309–313.
[12] J.H. Zhang, S.M. Xie, M. Zhang, M. Zi, P.G. He, L.M. Yuan, Novel inorganic mesoporous material with chiral nematic structure derived from nanocrystalline cellulose for high-resolution gas chromatographic separations, Anal. Chem. 86 (2014) 9595–9602.
[13] M.N. Hon, T.S. Lee, T.T. Tee, Extraction of cellulose nanocrystals from plant sources for application as reinforcing agent in polymers, Compos. Part B-Eng. 75 (2015) 176–200.
[14] D. Bondeson, A. Mathew, K. Oksman, Optimization of the isolation of nanocrystals from microcrystalline cellulose by acid hydrolysis, Cellulose 2 (2006) 171–180.
[15] L. Chen, R.M. Berry, K.C. Tam, Synthesis of β-cyclodextrin-modified cellulose nanocrystals (CNCs)@Fe_3O_4@SiO2 superparamagnetic nanorods, ACS Sustain. Chem. Eng. 2 (2014) 951–958.
[16] Y.S. Shin, G.G. Exarhos, Template synthesis of porous titania using cellulose nanocrystals, Mate. Lett. 61 (2007) 2594–2597.
[17] Y. Zhou, E.Y. Ding, W.D. Li, Synthesis of TiO_2 nanocubes induced by cellulose nanocrystal (CNC) at low temperature, Mater. Lett. 61 (2007) 5050–5052.
[18] K.E. Shopsowitz, H. Qi, W.Y. Hamad, M.J. MacLachlan, Free-standing mesoporous silica films with tunable chiral nematic structures, Nature 18 (2010) 422–426.
[19] J.L. Song, G.S. Fu, Q. Cheng, Bimodal mesoporous silica nanotubes fabricated by dual templates of CTAB and bare nanocrystalline cellulose, Ind. Eng. Chem. Res. 53 (2013) 708–714.
[20] S.H. Myoung, S.S. Im, S.H. Kim, Non-isothermal crystallization behavior of PLA/acetylated cellulose nanocrystal/silica nanocomposites, Polym. Int. 65 (2016) 115–124.
[21] N.C. Zhang, A.X. Yu, A.H. Liang, R.B. Zhang, F. Xue, E.Y. Ding, Preparation of SiC whisker and application in reinforce of polystyrene resin composite materials, J. Appl. Polym. Sci. 130 (2013) 579–586.
[22] M.A. El-Fattah, A.M.A. Hasan, M. Keshawy, A.M. El-Saeed, O.M. Aboelenien, Nanocrystalline cellulose as an eco-friendly reinforcing additive to polyurethane coating for augmented anticorrosive behavior, Carbohyd. Polym. 183 (2018) 311–318.
[23] V. Vardanyan, B. Poaty, G. Chauve, V. Landry, T. Galstian, B. Ried, Mechanical properties of UV-waterborne varnishes reinforced by cellulose nanocrystals, J. Coat. Technol. Res. 11 (2014) 841–852.
[24] M.Z. Pan, X.Y. Zhou, M.Z. Chen, Cellulose nanowhiskers isolation and properties from acid hydrolysis combined with high pressure homogenization, BioResources 8 (2013) 933–943.
[25] S. Suzuki, E. Ando, Abrasion of thin films deposited onto glass by the Taber test, Thin Solid Films 340 (1999) 194–200.
[26] F. Jiang, Y.L. Hsieh, Chemically and mechanically isolated nanocellulose and their self-assembled structures, Carbohyd. Polym. 95 (2013) 32–40.
[27] S.G. Iman, F. Khodaiyan, M. Mousavi, H. Yousefi, Preparation and characterization of nanocellulose from beer industrial residues using acid hydrolysis/ultrasound, Fiber Polym. 16 (2015) 529–536.
[28] O. Ander, S.E. Arantzazu, E. Arantxa, P.R. Cristina, A. Aitor, Office waste paper as cellulose nanocrystal source, J. Appl. Polym. Sci. 134 (2017) 45257–45267.
[29] T.J. Qu, X.M. Zhang, X.W. Gu, L.J. Han, G.Y. Ji, X.L. Chen, W.H. Xiao, Ball milling for biomass fractionation and pretreatment with aqueous hydroxide solutions, ACS Sustain Chem. Eng. 5 (2017) 7733–7742.
[30] E.A. Parvaneh, K. Mohammad, S. Gurvinder, Study of molecular conformation and activity-related properties of lipase immobilized onto core-shell structured polyacrylic acid-coated magnetic silica nanocomposite particles, Langmuir 32 (2016) 3242–3252.
[31] P. Cortes, T. Zhu, R. Guzman, G.B. Smith, Covalent coupling of polyacrylic acid coated magnetic-nanoparticles to multiwall carbon nanotubes for manipulation targets, J. Exp. Nanosci. 6 (2011) 665–678.
[32] Z. Qu, F. Hu, K. Chen, Z. Duan, H. Gu, H. Xu, A facile route to the synthesis of spherical poly(acrylic acid) brushes via RAFT polymerization for high-capacity protein immobilization, J. Colloid Interface Sci. 398 (2013) 82–87.
[33] J.A. Syed, H.B. Lu, S.C. Tang, Enhanced corrosion protective PANI-PAA/PEI multilayer composite coatings for 316SS by spin coating technique, Appl. Surf. Sci. 325 (2015) 160–169.
[34] P.C. Wang, Y.J. Hu, H.Q. Zhan, Vibrational spectroscopy of the mass-selected tetrahydrofurfuryl alcohol monomers and its dimers in gas phase using IR depletion and VUV single photon ionization, Spectrochim. Acta, Part A 185 (2017) 63–68.
[35] C.C. Chang, Y.T. Wu, L.P. Cheng, Preparation of HMDS-modified silica/polyacrylate hydrophobic hard coatings on PMMA substrates, J. Coat. Technol. Res. 13 (2016) 999–1007.
[36] J. Du, G.M. Zhao, M.Z. Pan, L.L. Zhuang, D.G. Li, R. Zhang, Crystallization and mechanical properties of reinforced PHBV composites using melt compounding: effect of CNFs and CNFs, Carbohyd. Polym. 168 (2017) 255–262.
[37] Y.Z. Wan, G.F. Zuo, F. Yu, Y. Huang, K.J. Ren, H.L. Luo, Preparation and mineralization of three-dimensional carbon nanofibers from bacterial cellulose as potential scaffolds for bone tissue engineering, Surf. Coat. Tech. 205 (2011) 2938–2946.